25
M

NASA TECHNICAL MEMORANDUM

NASA TM X-52361

NASA TM X-52361

CHAMBER SHAPE EFFECTS ON COMBUSTION INSTABILITY

by Harry E. Bloomer, John P. Wanhainen,
and David W. Vincent

Lewis Research Center
Cleveland, Ohio

TECHNICAL PAPER presented at Fourth Combustion Conference sponsored by the Interagency Chemical Rocket Propulsion Group
Menlo Park, California, October 2-13, 1967

NATIONAL AERONAUTICS AND SPACE ADMINISTRATION · WASHINGTON, D.C. · 1967

CHAMBER SHAPE EFFECTS ON COMBUSTION INSTABILITY

by Harry E. Bloomer, John P. Wanhainen, and David W. Vincent

Lewis Research Center
Cleveland, Ohio

TECHNICAL PAPER presented at

Fourth Combustion Conference
sponsored by the Interagency Chemical Rocket Propulsion Group
Menlo Park, California, October 2-13, 1967

NATIONAL AERONAUTICS AND SPACE ADMINISTRATION

E-4208

CHAMBER SHAPE EFFECTS ON COMBUSTION INSTABILITY

By Harry E. Bloomer, John P. Wanhainen,
and David W. Vincent

Lewis Research Center
National Aeronautics and Space Administration
Cleveland, Ohio

INTRODUCTION

Recent combustion instability studies at the NASA-Lewis Research Center were aimed at evaluating several techniques to suppress screaming in rocket combustors. Two dissimilar propellant combinations were used and gross differences in stability characteristics of each were compared. Most of the work reported here was done with the hydrogen-oxygen (H - O) combination. Earth-storable propellants (N_2O_4-50% N_2H_4-50% UDMH) were compared to hydrogen-oxygen in some instances. Stability rating was done with directional explosive charges for the storable propellants and varying the fuel injection temperature for the H-O combination.

Combustors were generally the same size in both cases; chamber diameter was 10.77 inches, contraction ratio was 1.9 and L^* was normally 42 inches. However, storable propellants were rated at a nominal chamber pressure of 100 psia and thrust of 6700 pounds as compared to 300 and 20,000, respectively, for the H-O combination. Variables studied were, (1) tapered chambers with concentrated pattern injectors, (2) injector precent radial coverage, (3) contraction ratio, (4) length of chamber sleeve, (5) spiral stepped sleeves and (6) nozzle shape. All experimental data are presented in Table I.

DISCUSSION

Some theoretical basis exists for changes in instability behavior with chamber shape. Priem's theory (Ref. 1) includes a burning rate parameter and a relative velocity term, which are affected by chamber shape. His theory suggests the use of a chamber with a contraction ratio less than one to increase the velocity difference between the injected liquid propellant and the surrounding gas. This should lead to increased stability relative to transverse modes. Experiments using hydrogen-oxygen propellants and earth storable propellants were designed to explore this possibility. Concentrated pattern injectors were run in cylindrical and two different half angle chamber configurations, as shown in figure 1. Presented in figure 2 are photos of the injectors used in the two phases of the test. The results for H-O are presented in figure 3. The hydrogen-oxygen data are presented as a function of mixture ratio and hydrogen injection temperature. The temperature limit boundary for the 15° tapered chamber could not be established because of facility limitation. However, it was unstable at temperatures higher than 240°R. The 30° tapered chamber was unstable at 140°R. In the cylindrical chamber, the concentrated pattern injector was unstable at 100°R. Therefore, the effect of high flow velocity seems to be destabilizing. A conventional 100 percent radial coverage injector with the same number of elements was stable down to temperatures as low as 60°R. This radial coverage variable will be treated later in the paper. The fact that the test did not follow the theory

TM X-52361

may be explained by the predominant mode of instability encountered. Shown in figure 4 are typical amplitude spectral density graphs for the three configurations run with hydrogen-oxygen propellants. As can be noted, the first longitudinal mode was predominant in all three configurations. The noticeable frequency shift with the tapered chambers was caused by the acoustic shortening phenomena.

The results from the storable test are presented in figure 5. The stability characteristics are presented in terms of bomb size and mixture ratio. The cylindrical chamber could be bombed unstable at high mixture ratio with charges varying from 45 down to 27 grains. The 30° taper chamber was spontaneously unstable at low mixture ratios from 1.49 to 1.71. The 15° taper chamber was completely stable over the entire mixture ratio range from 1.65 to 2.26 when bombed with 41 grain charges. The predominant modes observed in storable configurations were tangential. The result that the 15° taper chamber was more stable than either the 30° taper or cylindrical chamber is in agreement with Priem's theory.

Percent radial coverage of the injection pattern seemed to have a considerable effect on stability characteristics, so a test was devised to further explore this variable. Previous work during the F-1 development program also had shown an effect of face coverage. A theoretical treatment of this variable has been presented by Reardon, et al. (Ref. 2). His method uses distribution coefficients which are ascribed to each configuration. Their effect on a calculated pressure interaction index then was interpreted in terms of stability. In this investigation, four 397 concentric tube element injectors were designed to have 60, 72, 85, and 100% radial coverage of the injection patterns. The results of this test with hydrogen-oxygen propellants are presented in figure 6.

It should be noted that the most stable injector had 100% coverage. The curve through the data points reaches a maximum (or least stability) at a coverage of about 75% and then decreases again (becomes more stable) as coverage decreases. The 60% configuration exhibited unusual characteristics during the hydrogen temperature ramp. First radial mode of instability was encountered first at a hydrogen injection temperature of 125°R. As the temperature decreased to 108°R, the first tangential mode was the only mode identified. This change of predominant mode to radial as injection patterns become concentrated toward the center has been previously reported by Purdue's Jet Propulsion Laboratory (Ref. 3).

Another injector configuration of 200 elements was made less stable by simply welding closed the outside row of 43 elements to decrease the percent coverage from 100 to 75. This resulted in an increase of approximately 50°R in the transition hydrogen injection temperature. Based on this result, a 400 element triplet injector used with earth storables was tested and then modified by welding closed the outer row of 68 elements. The stability test results in terms of bomb size and mixture ratio are presented in figure 7. At mixture ratios above 1.6, the stability was decreased by decreasing the percent coverage from 90 to 70. These results are consistent with the hydrogen-oxygen results of figure 6, but do not agree with results obtained elsewhere. It is postulated that a strong recirculation exists in the void zone which brings hot gases into the area where the propellant is introduced and the result may then be similar to swirl or gas injection rating techniques used to induce instability. Recirculation could be the controlling factor until the void zone becomes large enough so that the normal distribution theory becomes controlling - at about 78% radial coverage.

The next logical step was the testing of the 4 hydrogen-oxygen injectors used on the radial coverage experiment with full length spools in the combustion chamber to provide 100% radial coverage for varying chamber diameters. A test of this type with the chamber pressure and nozzle throat area held constant means a variation in combustion chamber gas velocity, as well as contraction ratio. The results are presented in figure 8 in terms of hydrogen transition temperature and contraction ratio at a mixture ratio of 5.0. The transition to unstable combustion occurred at about 65°R for all four cases. All four experienced first tangential instability. The contraction ratio varied from 1.1 to 1.9 for these data and there was no effect of contraction ratio as long as thrust and total weight flow were kept constant.

The effect of varying contraction ratio by changing the nozzle throat area and keeping the same injector and chamber cross section areas is presented in figure 9. In this test series, the chamber pressure was held constant at 300 psia and the weight-flow-per-element was allowed to vary with contraction ratio. The results indicate that increasing contraction ratio from 1.5 to 4.5 is destabilizing to a tangential mode proclivity. For this particular 421 element injector with an 85% radial pattern coverage, the hydrogen transition temperature was increased from 118°R to 242°R at a mixture ratio of 5.0. Other tests which varied chamber pressure and kept weight-flow-per-element constant did not change the hydrogen temperature at instability transition from these results. No attempt will be made here to present the theoretical treatment of these effects of contraction ratio, chamber pressure and weight flow. These are explained by Feiler in reference 4 using the response factor model. It is evident from the results of this phase of the investigation that the designer can scale thrust (upwards) by increasing throat diameter (decreasing contraction ratio) and flow rate not only without a loss in stability but with an improvement in hydrogen temperature stability margin. In fact, increasing the nozzle throat diameter may possibly be a useful technique to improve the stability of an existing marginally stable hydrogen-oxygen engine.

The 60% radial pattern coverage injector was tested with a series of chamber blocks or sleeves. These tests were initiated with a view to finding how short chamber-sleeves could be made and still have a stabilizing effect. The results are presented in figure 10, in terms of sleeve length and hydrogen injection temperature. The effective contraction ratio from the sleeve inner diameter to the throat was 1.14. A 4-inch long sleeve was equivalent to a full length sleeve in its stabilizing effect, with a common transition temperature of about 65°R. The predominant mode of instability was either second tangential inside the sleeve or first radial in the 10.8-inch diameter. As the length was decreased below 2 inches, the stabilizing effect was lessened rapidly. The 60% coverage point at 0 sleeve length was taken from the previous series of coverage tests. The transition temperature indicated is a transition to the first radial mode which is consistent with the 60% coverage results presented earlier with no sleeves. The dashed line indicating the onset of instability for the tapered sleeve configuration seems to be an anomaly since it actually results in decreased stability.

A variation of the sleeve configuration is the spiral stepped sleeve. A sketch of this sleeve and the stability results are presented in figure 11. The purpose of the sleeve was to interfere with spinning waves. It was 3 inches long and covered the radial pattern of the injector from a value of 60% to 100%. It should have yielded stability characteristics similar to a 3-inch long sleeve of about 80% coverage only if the wave interference did not work. Shown on figure 11 is a line indicating the level of stability of an 80% coverage full length sleeve. Keeping in mind from figure 10 that a 3-inch long sleeve would have a transition temperature slightly higher than a full length sleeve, the spiral sleeve actually contributed more stability than a 3-inch, 80% sleeve. At a mixture ratio of 5.0, the transition temperature was 95°R, compared to a value of about 133° for a full length 80% coverage sleeve.

Analytical effect on stability of variations in nozzle shape has been reported by the group from Princeton (Ref. 5). This part of the investigation was an examination of the possibility of improving tangential mode stability characteristics (minimum stable hydrogen temperature) of the combustor by increasing acoustic flow losses through the exhaust nozzle. It was hypothesized that, at the hydrogen temperature screech boundary, a state exists where the acoustic energy gains equal the acoustic energy losses of the combustor. An increase, therefore, in acoustic energy losses should result in lowering the minimum stable hydrogen temperature. Tests of several nozzle configurations were made with hydrogen-oxygen propellants. The results of the tests are presented in figure 12. All the chambers shown on the figure experienced tangential mode instability. No change in stability characteristics are discernible, although data scatter are greater than is usual.

Results of reference 6 indicate that flow dependent losses through a vent (nozzle) increase as the vent is moved toward the pressure antinode. In this case, tangential mode instability, the pressure antinode is at the walls of the combustor; thus, for maximum losses, the nozzle open area should be positioned at the periphery of the combustor. Accordingly, a nozzle was fabricated with an internal plug and eight radial support spokes (wagon wheel) as shown in figure 13. The nozzle was evaluated with a 421-element concentric tube injector and a cylindrical combustion chamber.

The stability characteristics of a combustor with a conventional convergent-divergent nozzle and the annular flow (wagon wheel) nozzle are compared in figure 14. The hydrogen temperature stable operating limits were improved about 20°R with the wagon wheel nozzle compared to the conventional configuration. The limited success of the wagon wheel configuration may be due to its distant location from the region of highest energy release (maximun screech amplitude) which normally occurs near the injector (Ref. 7). The general conclusion to be drawn from this phase of the work is that drastic changes in nozzle shape appear to be of little help in improving stability of a hydrogen-oxygen chamber.

SUMMARY OF RESULTS OF CHAMBER SHAPE EFFECTS ON SCREECH CHARACTERISTICS

1. Concentrating the combustion process using tapered chambers and a concentrated pattern injector had a detrimental effect on the longitudinal mode of screech, although stability was improved when a tangential instability was the predominant mode.

2. Concentration of the elements of an injector in 75% of the face area resulted in a higher hydrogen temperature transition into tangential instabilith than either a greater or a lesser radial coverage.

3. Variation in contraction ratio from 1.1 to 1.9 by changing the chamber diameter and keeping the injection pattern radial coverage and nozzle throat diameter constant did not affect the transition temperature of the tangential mode.

4. Decreasing contraction ratio from 4.5 to 1.5 by increasing exhaust nozzle area had a stabilizing effect on tangential mode instability.

5. A partial length (4") chamber sleeve had the same effect as a full length sleeve on stability. Shorter lengths contributed less stabilization and the effect became the same as the radial coverage effect when the sleeve length approached zero.

6. A spiral sleeve (3" long) contributed some stability to the system.

7. The admittance or sharp orifice nozzle had essentially no effect on stability when compared to a conventional smooth transition nozzle.

8. The plug or wagon wheel nozzle provided a slight improvement on tangential mode stability.

E-4208

REFERENCES

1. Priem, Richard J.; and Guentert, Donald C.: Combustion Instability Limits Determined by a Nonlinear Theory and a One-Dimensional Model. NASA TN D-1409, 1962.

2. Reardon, F. H.; McBride, J. M.; and Smith, A. L., Jr.: Effect of Injection Distribution on Combustion Stability. AIAA J., vol. 4, no. 3, Mar. 1966, pp. 506-512.

3. Zucrow, M. J.; Osborn, J. R.; and Bonnell, J. M.: High Frequency Combustion Pressure Oscillations in Motors Burning Gaseous Propellants. Rep. No. JPC-409, TM-65-5, Purdue University, Aug. 1965.

4. Feiler, Charles E.: Effect of Combustor Parameters on the Stability of a Gaseous Hydrogen - Liquid Oxygen Engine. Paper presented at Fourth Combustion Conference, Interagency Chemical Rocket Propulsion Group, Oct. 2-13, 1967.

5. Crocco, L.; Harrje, D. I.; and Sirignano, W. A.: Nonlinear Aspects of Combustion Instability in Liquid Propellant Rocket Motors. Second Combustion Conference, Interagency Chemical Rocket Propulsion Group, Vol. 1. CPIA Publ. No. 105, Applied Physics Lab., Johns Hopkins Univ., May 1966, pp. 63-105.

6. Gordon, Colin; and Smith, P. W., Jr.: Acoustic Losses of a Resonator with Steady Gas Flow. J. Acoust. Soc. Am., vol. 37, no. 2, Feb. 1965, pp. 257-267.

7. Clayton, R. M.; and Rogero, R. S.: Experimental Measurements on a Rotating Detonation-like Wave Observed During Liquid Rocket Resonant Combustion. Tech. Rep. 32-788 (NASA CR-67259), Jet Propulsion Lab., California Inst. Tech., Aug. 15, 1965.

TABLE I. - EXPERIMENTAL DATA

Figure number	Test	Chamber diameter at injector, in.	Largest chamber diameter, in.	Throat diameter, in.	Percent coverage of injection elements	Contraction ratio, A	$(H_2 - O_2)$ or storables	Number of injection elements	Static pressure at injector, psia	Fuel weight flow, W_f, lb/sec	Oxidant weight flow, W_o, lb/sec	Oxidant-fuel ratio, O/F	Efficiency of characteristic exhaust velocity, η_c^*, percent	Fuel injection temperature, °R	Bomb size required to drive, grains	Stability classification	Chamber taper half angle, deg
Taper chamber studies																	
5	722	10.78	10.78	7.82	12	1.9	$H_2 - O_2$	100	---	11.3	56.1	4.95	-----	99	----	Transition	0
	723	10.78			--	1.9			---	10.9	54.8	5.01	-----	97	----		0
	724	10.78			--	1.9			---	12.1	50.4	4.15	-----	85	----		0
	719	3.97			85	0.257			---	10.9	45.5	4.15	-----	106	----		30
	720								398	10.4	52.1	5.03	-----	125	----		30
	721								418	10.3	53.5	5.20	-----	131	----		30
	773								663	10.9	46.9	4.31	-----	238	----	Unstable	15
	774								678	10.2	52.6	5.18	-----	249	----	Unstable	15
4	65	10.78			--	1.9	Storables	50	109.9	9.25	18.50	2.00	96.13	542.6	Damp		30
	66				--				108.3	9.27	18.58	2.0	96.34	543.6	Damp		
	67				--				108.2	9.30	18.62	2.0	96.21	543.2	Damp		
	68				--				108.2	9.96	17.02	1.71	96.30	544.6	Spontaneously		
	69				--				110	9.82	17.79	1.81	96.84	542.3	Damp		
	70				--				113	10.50	16.87	1.61	97.54	545.5	Spontaneously		
	153				--				126	10.40	20.16	1.94	96.91	539.3	Damp		
	154				--				132	10.44	22.65	2.17	96.42	530.3	40.81		
	155				--				125	11.54	17.26	1.49	97.30	528.8	Damp		
	156				--				125	10.50	19.37	1.84	97.44	528.9	27.79		
	79				--				133.9	10.18	18.60	1.83	99.2	544.3	Damp		15
	81				--				130.2	10.37	17.06	1.65	98.1	542.7			
	82				--				132.5	9.98	18.87	1.89	97.9	541.6			
	140				--				125	8.96	20.31	2.26	97.08	515.6			
	141				--				130	9.86	18.88	1.91	97.85	514.3			
	142				--				131	9.57	20.34	2.12	97.85	512.9			
	[a]89				90			400	105	9.65	18.59	1.93	97.93	536.3	1.63		Cylindrical
	[a]90								107	11.04	16.65	1.51	98.53	538.2	Spontaneously		
	[a]91								104	8.89	19.66	2.21	97.3	535.6	1.63		
	[a]93								106	9.71	18.94	1.95	98.4	536.1	1.63		
	109				--			50	126	10.01	20.11	2.01	97.46	541.6	40.81		
	110				--				132	11.26	18.73	1.665	99.0	539.7	Damp		
	111				--				111	8.43	21.36	2.53	94.55	540.6	27.79		
	125				--				111	9.64	17.8	1.84	96.94	530.8	32.15		
	126				--				119	9.99	19.25	1.93	97.16	528.9	45.23		
	127				--				118	9.45	20.65	2.19	96.26	525.1	23.43		
	128				--				118	9.38	20.68	2.20	96.28	524.5	23.43		
	129				--				126	10.59	19.67	1.86	97.64	527.3	Damp		
	[a]214				70			332	109	10.17	20.12	1.97	97.73	525.7	Spontaneously		
	[a]215				70			332	102	8.78	20.57	2.34	96.82	528.3	Spontaneously		
	[a]216				70			332	110	11.50	18.38	1.60	97.93	527.4	Spontaneously		

[a] Runs also used for fig. 7. - Effect on injection pattern radial coverage.

TABLE I - Continued. - EXPERIMENTAL DATA

Figure number	Test	Chamber diameter at injector, in.	Largest chamber diameter, in.	Throat diameter, in.	Percent coverage of injection elements	Contraction ratio, A	(H_2 - O_2) or storables	Number of injection elements	Static pressure at injector, psia	Fuel weight flow, W_f, lb/sec	Oxidant weight flow, W_o, lb/sec	Oxidant-fuel ratio, O/F	Efficiency of characteristic exhaust velocity, η_{c^*}, percent	Fuel injection temperature, °R	Bomb size required to drive, grains	Stability classification	Chamber taper half angle, deg
Injection pattern radial coverage																	
6	[a]292	10.764	10.78	7.83	100	1.9	H_2 - O_2	397	317	10.09	48.92	4.85	102.0	114	---	Stable	
	[a]293								---	------	------	----	---	---	---		
	[a]294								346	11.56	55.90	4.84	97.3	63.3	---	Transition	
	[a]295								326	13.42	51.45	3.83	93.1	65.4	---		
	[a]296								338	10.28	58.29	5.67	96.1	63.3	---		
	[a]297								335	9.90	61.25	6.17	93.5	61.9	---		
	[b]347	8.341	10.78		60				296	9.94	51.33	5.16	92.9	122	---		
	[b]348								301	11.44	46.98	4.09	94.1	105	---		
	[b]349								314	8.10	55.25	6.82	101.2	181	---		
	[b]350								310	8.06	55.31	6.86	100.0	166	---		
	[b]351								312	10.54	49.47	4.69	98.7	122	---		
	[b]352								314	8.81	54.23	6.16	99.4	151	---		
	[b]353								303	9.62	50.88	5.29	98.5	129	---		
	358	9.924	10.78		85				299	9.60	48.28	5.03	99.0	118	---	Transition	
	359								---	-----	-----	----	----	----	---	----------	
	360								306	13.63	44.19	3.24	98.5	105	---	Stable	
	361								299	11.30	45.26	4.01	98.9	111	---	Transition	
	362								316	8.57	55.78	6.51	99.3	169	---		
	363								297	8.90	50.39	5.66	98.4	145	---		
	364								296	10.27	47.30	4.61	97.3	118	---		
	365								296	8.35	52.31	6.26	97.9	148	---		
	546	9.138	10.78		72				319	12.25	46.84	3.82	109.2	136	---	Stable	
	547								311	12.20	47.30	3.88	97.2	121	---	Transition	
	548								316	10.36	57.25	4.95	97.9	141	---		
	549								317	9.32	54.78	5.89	97.4	153	---		
	550								315	11.59	49.83	4.30	96.3	127	---		
	551								317	9.64	54.58	5.66	96.7	147	---		
Contraction ratio																	
8	772	9.90	10.78	7.82	100	1.61	H_2 - O_2	397	314	10.93	48.85	4.47	98.2	64.3	---	Transition	
	773								313	9.35	50.76	5.43	100.4	61.9	---	Stable	
	774								293	9.24	52.97	5.73	91.8	68.2	---	Unstable	
	775								312	8.71	52.12	5.98	100.9	62.5	---	Transition	
	776								313	12.45	44.99	3.62	99.9	59.6	---	Stable	
	369	8.341	8.35			1.138			297	11.31	43.16	3.82	88.0	65.5	---	Transition	
	370								296	9.80	46.18	4.71	90.64	71.2	---	Transition	
	371								314	9.64	53.56	5.55	87.70	58.5	---	Stable	
	372								315	10.62	49.96	4.70	89.21	58.0	---	Stable	
	373								318	12.81	47.04	3.67	88.7	57.6	---	Stable	

[a] Runs also used for fig. 8. - Effect of contraction ratio.
[b] Runs also used for fig. 10. - Effect of chamber sleeve length.

TABLE I - Continued. - EXPERIMENTAL DATA

Figure number	Test	Chamber diameter at injector, in.	Largest chamber diameter, in.	Throat diameter, in.	Percent coverage of injection elements	Contraction ratio, A	($H_2 - O_2$) or storables	Number of injection elements	Static pressure at injector, psia	Fuel weight flow, W_f, lb/sec	Oxidant weight flow, W_o, lb/sec	Oxidant-fuel ratio, O/F	Efficiency of characteristic exhaust velocity, η_c^*, percent	Fuel injection temperature, °R	Bomb size required to drive, grains	Stability classification	Chamber taper half angle, deg
Contraction ratio - Continued																	
8	552	9.138	9.15	7.82	100	1.367	$H_2 - O_2$	397	307	10.39	51.89	4.99	89.1	64.7	---	Transition	
	553								304	11.96	46.97	3.93	90.6	64.7	---		
	554								311	9.65	53.34	5.53	90.9	64.0	---		
	555								319	11.74	50.97	4.34	90.1	62.3	---		
	556								318	9.55	54.46	5.70	92.3	62.6	---		
9	255	9.935	10.78		85	3.0		421	278	5.93	30.94	5.21	96.1	196	---		
	256								287	7.24	28.09	3.88	99.9	133	---		
	257								288	5.79	33.45	5.78	95.4	244	---		
	258								310	7.13	31.22	4.38	100.2	149	---		
	259								301	6.72	31.32	4.66	99.0	167	---		
	290								271	5.31	32.57	6.13	-----	233	---		
	291								275	7.99	29.38	3.67	-----	130	---		
	292								320	8.37	29.22	3.49	101.5	124	---	Stable	
	293								307	6.66	31.55	4.74	98.2	164	---	Transition	
	294								316	6.52	34.51	5.29	95.8	199	---		
	274					4.5			316	4.01	24.10	6.00	96.9	351	---	Stable	
	275								317	4.37	25.20	5.76	91.7	270	---	Transition	
	277								315	4.79	23.40	4.89	93.2	230	---		
	279								315	5.27	21.30	4.03	96.9	174	---		
	280								316	5.22	22.90	4.40	92.2	191	---		
	281								316	4.32	28.10	6.49	-----	354	---		
	282								316	5.30	27.30	5.16	-----	242	---		
	326					1.5			346	13.79	66.20	4.80	98.7	115	---		
	327								354	12.45	69.98	5.62	100.6	126	---		
	328								327	13.74	60.30	4.39	99.7	109	---		
	329								351	12.87	68.91	5.35	99.6	122	---		
	330								348	12.92	70.66	5.47	97.1	121	---		
	331					1.9			332	12.69	48.36	3.81	100.3	112	---		
	333								358	11.06	56.51	5.11	100.9	135	---		
	335								339	9.61	55.86	5.81	101.0	164	---	Stable	
	336								329	11.20	50.30	4.51	100.1	120	---	Transition	
	337								340	10.41	53.98	5.18	100.8	136	---		
Chamber sleeve length																	
10	441	8.35	10.78	7.82	60	1.9	$H_2 - O_2$	397	319	10.74	50.76	4.73	99.5	103	---	Transition	
	442								311	11.92	45.19	3.79	110	95	---		
	443								318	9.53	54.01	5.67	99.3	120	---		
	444								311	11.08	47.10	4.25	101	101	---		
	445								318	10.03	51.99	5.18	99.7	122	---		
	429								318	10.07	48.08	4.77	104	81	---		
	431								305	11.85	45.16	3.81	99.6	74	---		
	432								302	9.25	55.41	5.99	92.4	61.5	---	Stable	
	433								---	-----	-----	----	-----	----	---	------	
	434								319	11.03	47.26	4.28	102	77	---	Transition	
	435								305	9.42	48.91	5.19	101	97.6	---		
	424								309	10.07	48.50	4.81	100.5	76	---		
	425								325	12.54	47.09	3.75	101.4	67	---		
	426								296	8.89	51.84	5.83	96.4	83.1	---		

TABLE I - Concluded. - EXPERIMENTAL DATA

Figure number	Test	Chamber diameter at injector, in.	Largest chamber diameter, in.	Throat diameter, in.	Percent coverage of injection elements	Contraction ratio, A	($H_2 - O_2$) or storables	Number of injection elements	Static pressure at injector, psia	Fuel weight flow, W_f, lb/sec	Oxidant weight flow, W_o, lb/sec	Oxidant-fuel ratio, O/F	Efficiency of characteristic exhaust velocity, η_{c^*}, percent	Fuel injection temperature, °R	Bomb size required to drive, grains	Stability classification	Chamber taper half angle, deg
Chamber sleeve length - Continued																	
10	427	8.35	10.78	7.82	60	1.9	$H_2 - O_2$	397	320	13.53	44.73	3.30	101.7	58.9	---	Stable	
	428								314	9.84	51.37	5.22	99.1	77	---	Transition	
	383								303	10.39	43.47	4.19	95.8	82.8	---	Stable	
	384								308	10.18	48.38	4.75	90.7	68.1	---	Transition	
	385								307	11.73	44.48	3.79	91.6	65.6	---		
	386								298	9.16	52.84	5.77	85.9	67.4	---		
	436								303	11.01	53.22	4.84	89.8	71	---		
	437								305	12.80	49.40	3.86	91.2	66.3	---		
	438								298	9.71	56.43	5.81	88.8	77	---		
	439								302	12.16	52.10	4.28	88.2	69	---		
	440								300	10.66	55.98	5.25	86.9	70	---		
Spiral stepped sleeve																	
11	392	8.341	10.78	7.82	60	1.9	$H_2 - O_2$	397	304	10.09	47.87	4.74	97.8	100	---	Transition	
	393								304	11.73	44.70	3.77	99.4	93	---		
	394								304	8.93	51.43	5.76	97.5	106	---		
	395								302	10.86	46.31	4.26	97.4	93	---		
	396								302	9.61	50.14	5.22	95.9	103	---		
	397								303	9.62	50.20	5.22	96.7	100	---		
Nozzle shape effect																	
12	822	9.935	10.78	7.82	85	3.0	$H_2 - O_2$	421	313	5.84	31.64	5.23	107.6	188.7	---	Stable	
	823								319	6.26	31.98	5.08	104.3	158.4	---	Transition	
	824								311	5.97	31.23	5.23	104.5	158.0	---		
	825								317	6.32	33.16	5.25	100.5	166	---		
	826								311	6.51	34.33	4.99	99.1	164	---		
	827								303	6.05	32.14	5.09	102.5	209	---		
	828								313	7.19	32.27	4.44	97.7	208	---	Unstable	
	829								313	6.16	32.63	5.14	103.2	184	---	Transition	
	830								310	6.78	35.01	4.92	95.61	194	---		
	831								311	6.93	36.12	4.96	93.25	191	---		
	832								307	7.76	32.11	4.03	95.16	132	---		
	833								308	5.74	35.96	5.93	99.27	280	---	Stable	
Wagon wheel nozzle																	
14	30	9.935	10.78	7.82	85	1.9	$H_2 - O_2$	421	277	9.9	51.6	5.17	90.9	119	---	Transition	
	31								289	11.8	48.3	4.09	94.4	90	---		
	32								271	9.2	54.9	5.96	87.7	120	---		
	33								298	11.0	51.4	4.65	95.2	111	---		
	34								286	9.9	53.4	5.36	91.7	105	---		

E-4208

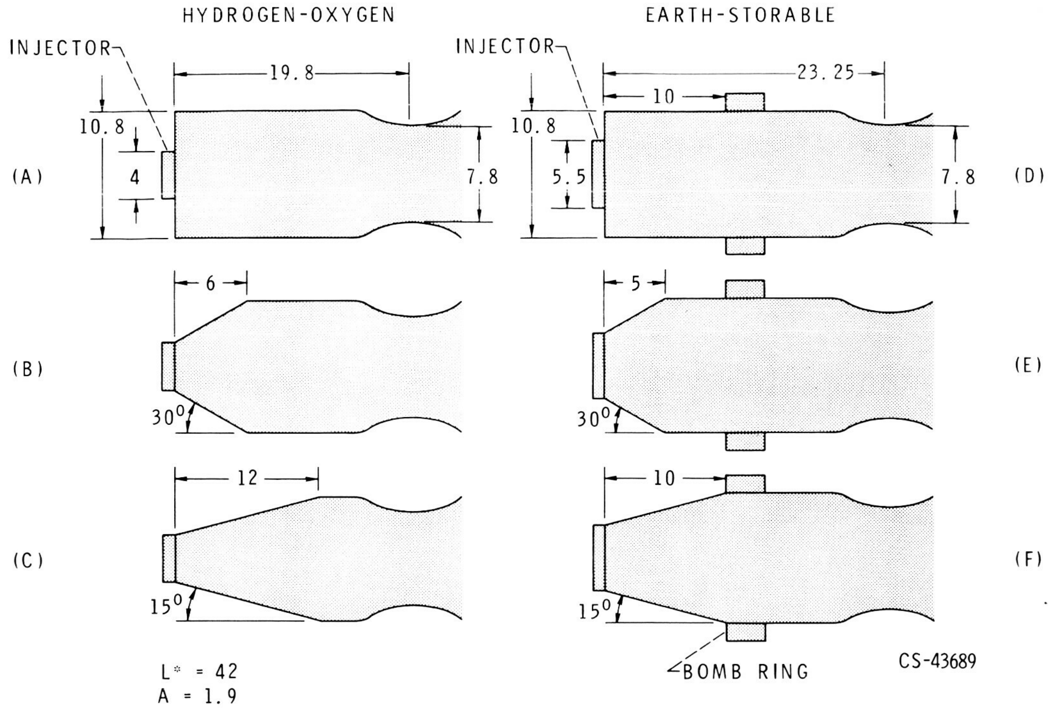

Figure 1. - Chamber shape variations.

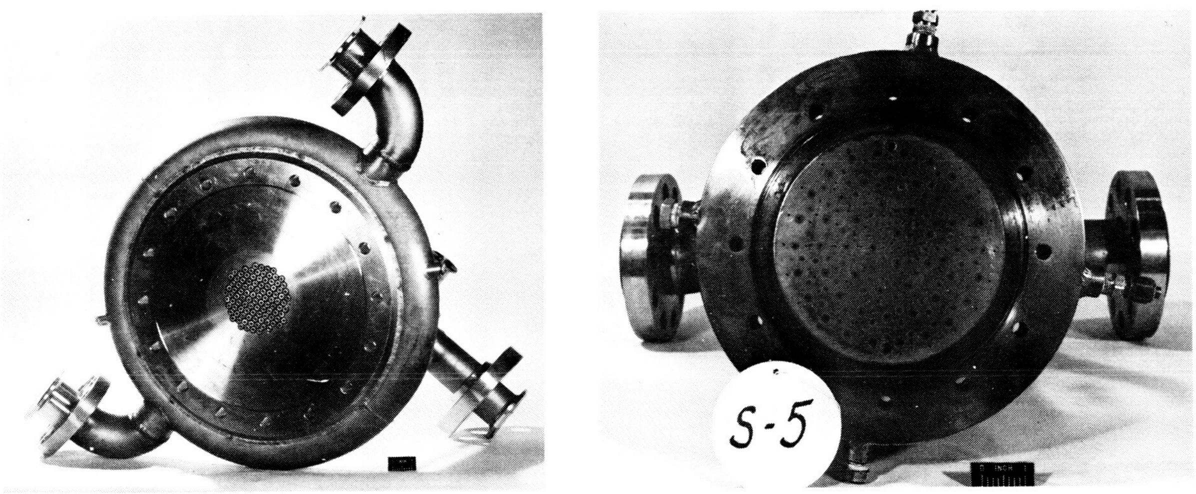

(A) HYDROGEN-OXYGEN INJECTOR (100 ELEMENTS). (B) STORABLE INJECTOR (50 ELEMENTS).

CS-43691

Figure 2. - Injectors used in injection concentration studies.

E-4208

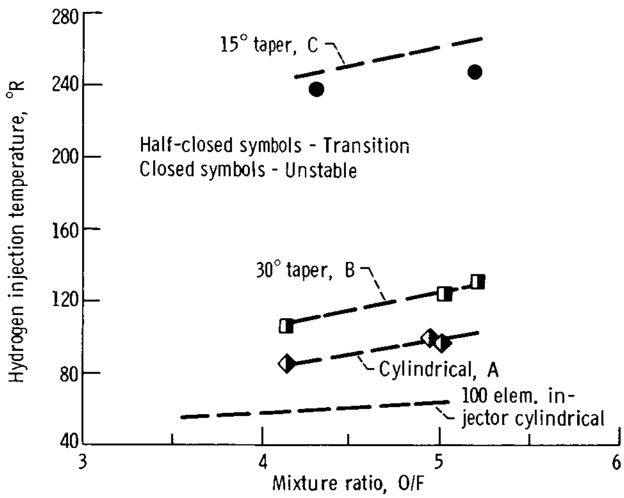

Figure 3. - Chamber shape results. Hydrogen-oxygen propellants, P_c = 300 psia; thrust = 20 K.

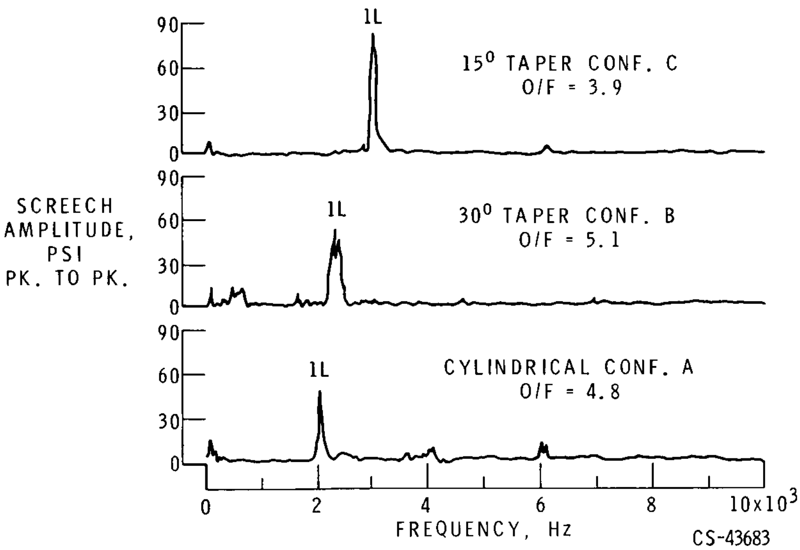

CS-43683

Figure 4. - Chamber shape spectral density traces, concentrated pattern injector. Hydrogen-oxygen propellants, P_c = 300 psi.

E-4208

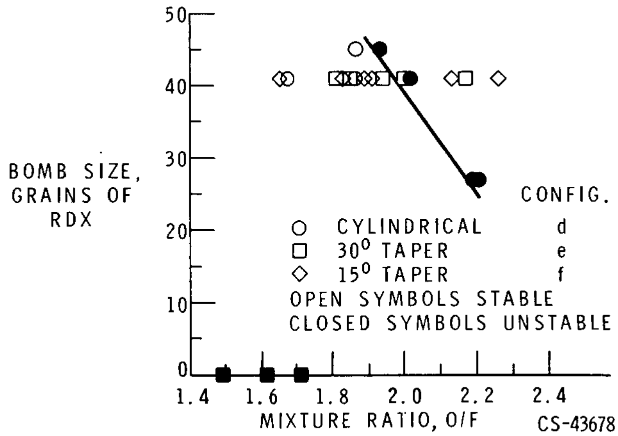

Figure 5. - Chamber shape results. Earth storable propellants, P_c = 100 psia; thrust = 6.7 K.

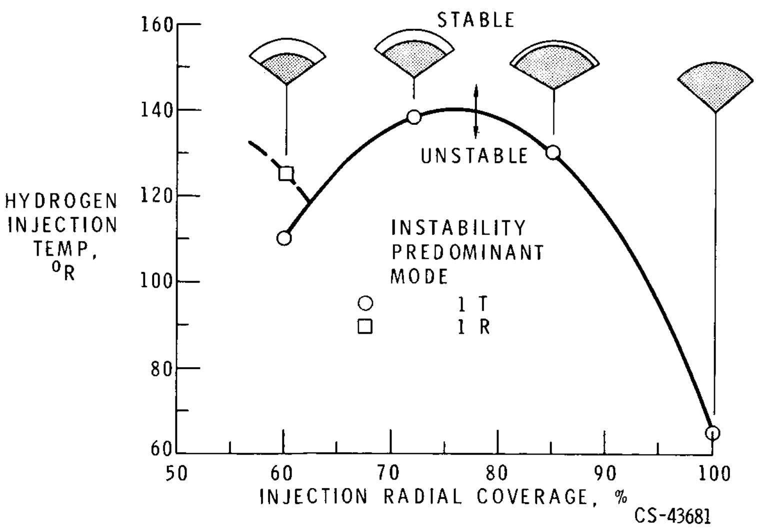

Figure 6. - Effect of injection pattern radial coverage. Hydrogen-oxygen propellants, P_c = 300 psia; O/F = 5.0; 397 element injectors.

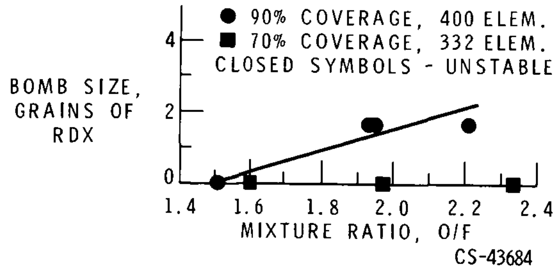

Figure 7. - Effect of injection pattern radial coverage. Storable propellants, P_c = 100 psia.

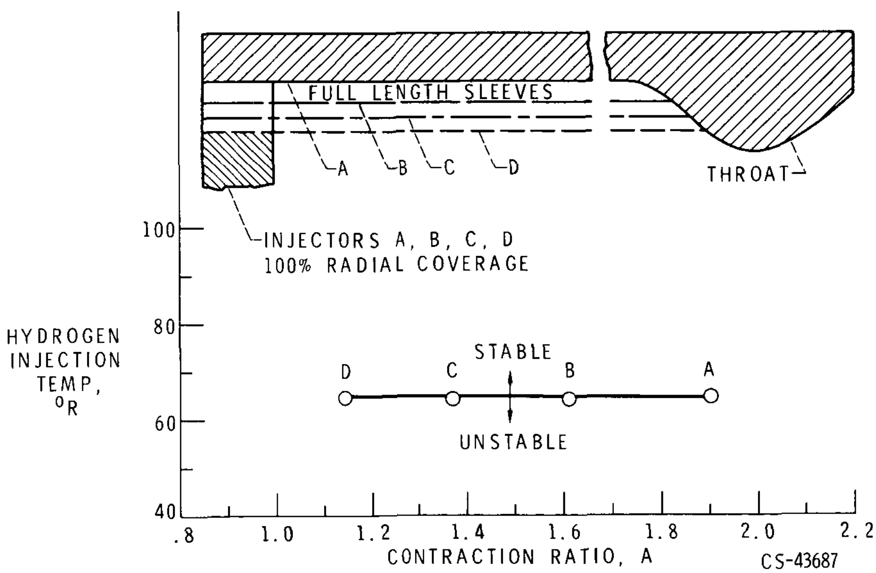

Figure 8. - Effect of contraction ratio. Hydrogen-oxygen propellants, P_c = 300 psi; O/F = 5.0.

E-4208

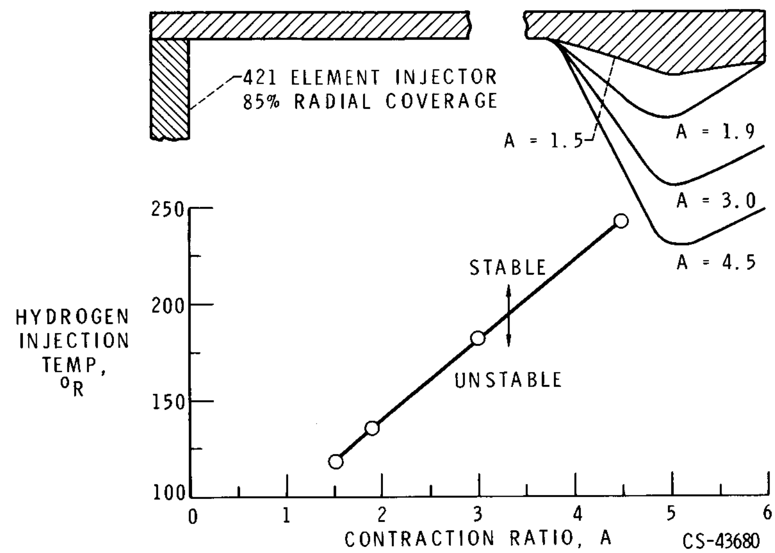

Figure 9. - Effect of contraction ratio. Hydrogen-oxygen propellants, P_c = 300 psi; O/F = 5.0.

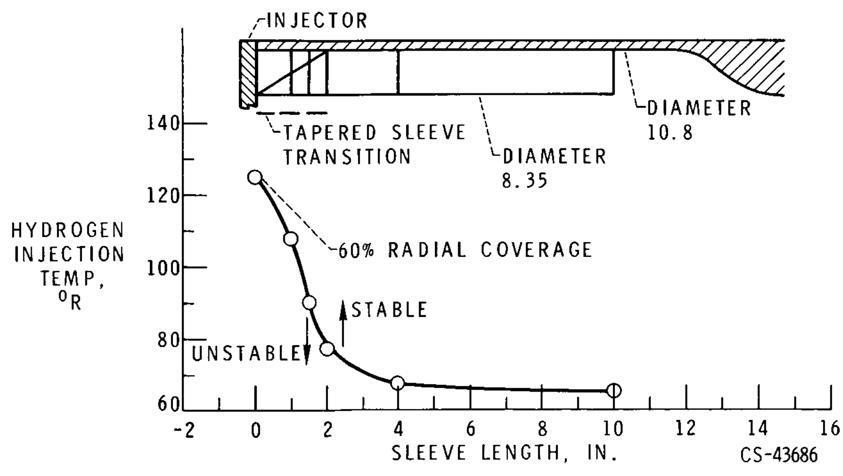

Figure 10. - Effect of chamber sleeve length. Hydrogen-oxygen propellants, P_c = 300 psia; O/F = 5.0; A = 1.9 without sleeves.

E-4208

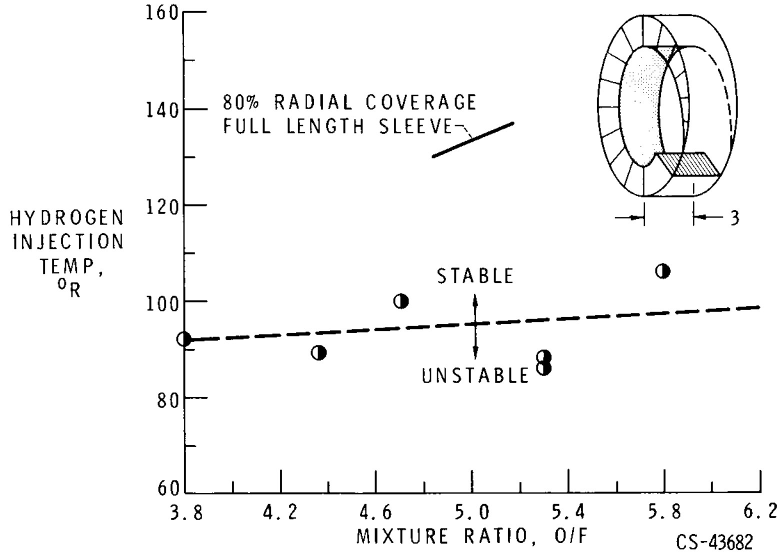

Figure 11. - Effect of spiral stepped sleeve. Hydrogen-oxygen propellants, P_c = 300 psia.

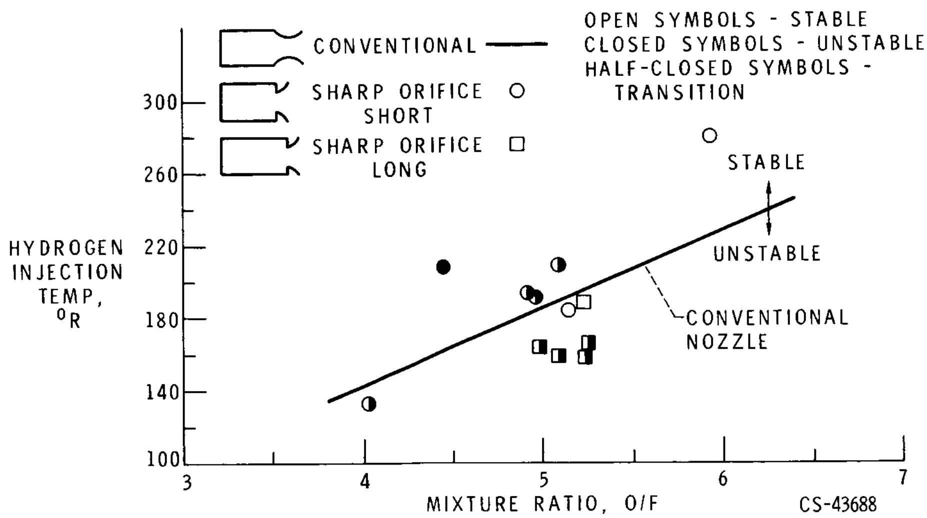

Figure 12. - Nozzle shape effect on stability. Contraction ratio = 3.0, P_c = 300 psia.

E-4208

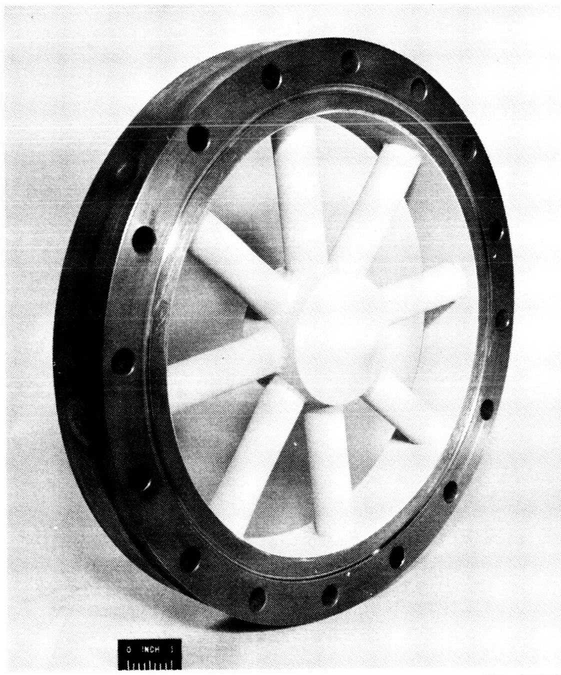

CS-43690

Figure 13. - Photo of "Wagon" wheel nozzle.

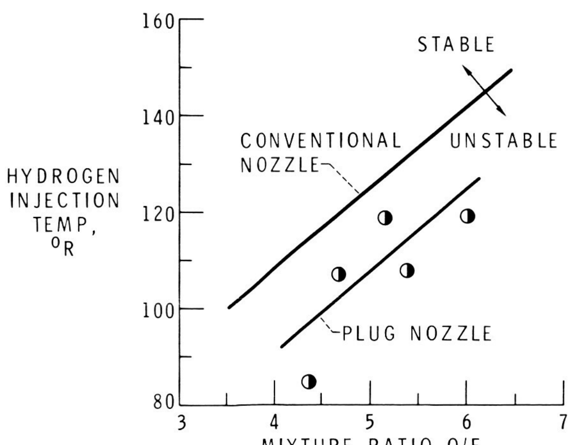

CS-43677

Figure 14. - Effect of nozzle shape. Hydrogen-oxygen propellants, P_c = 300 psia.